Journal of Polymers and the Environment (2022) 30:2847–2861
https://doi.org/10.1007/s10924-022-02404-6

ORIGINAL PAPER

Synthesis and Characterization of Dual-ion-Crosslinked Magnetic Sodium Alginate-Based Fe-SA-Y@Fe_3O_4 Biogel Composite with Ultrastrong Performance for Azo Dye Removal

Beigang Li[1,2] · Ting Lv[1,2] · Yanlong Shen[1,2]

Accepted: 9 February 2022 / Published online: 18 February 2022

Abstract

Magnetic sodium alginate(SA)-based biogel composite Fe-SA-Y@Fe_3O_4 macroparticles were synthesized by co-crosslinking of Y(III) and Fe(III) ions according to the optimized preparation conditions and characterized by various modern analytical techniques. The results show that the macrogel beads have unique cauliflower-shaped surface and sensitive magnetic response. Fe-SA-Y@Fe_3O_4 composite was used for the removal of Direct Red 13 (DR 13) and Direct Black 19 (DB 19) dyes from water. The adsorption capacities and removal efficiency can reach 2487 mg/g and 99.5% for DR-13 and 2992 mg/g and 99.7% for DB-19 respectively within the equilibrium time of 60 min at 298 K and pH 2.0, and decrease slightly with pH up to 10.0. The kinetic and equilibrium adsorption data followed the Pseudo-second-order rate model and Langmuir isothermal model well, respectively. Electrostatic adsorption, various H-bonding and complexation were largely involved in dye adsorption processes with spontaneous and exothermic character by macrogel beads, which were explained by thermodynamic studies, X-ray photoelectron spectroscopy (XPS) and Fourier transform infrared spectroscopy (FTIR), respectively. Fe-SA-Y@Fe_3O_4 composite with ultrahigh adsorption capacity and fast magnetic separation property will be a promising eco-friendly bio-based adsorbent for the superefficient purification of practical azo-dye effluents.

Keywords Sodium alginate · Yttrium(III)-Iron(III) ions · Azo dyes adsorption · Magnetism · Biogel composite

Introduction

One of the main causes of environmental water pollution and harm to human health is the discharge of a large number of organic dyestuff wastewater produced in various industrial processes without treatment or incomplete pretreatment [1]. Familiar azo dyes are the most widely used synthetic dyes in the production and daily life [2]. However, azo dyes in discharged effluents with high salinity and ecotoxicity [3] can be decomposed to produce more than 20 aromatic amines under special conditions, which may cause mutagenicity, teratogenicity and carcinogenicity [4, 5]. Direct Red 13 (DR 13) and Direct Black 19 (DB 19), belonging to disazo and polyazo dyes, have been widely used for direct dyeing in producing industries of cellulose fibers, cotton, silk, leather, viscose and so on because of their cheapness, good water solubility, color diversity, simplicity and directness of dyeing [6]. Nevertheless, these dyes are difficult to discolor, weakly biodegradable and potentially toxic due to their complex aromatic ring structures. This has prompted the ceaseless research and development of various new water treatment technologies for effective removal of azo dyes from wastewater, but among which, adsorption technology has been universally acknowledged as the most commonly used, the most economical, highly efficient, the fastest and easiest method to operate. Moreover, various types of adsorbents can be prepared by many different raw materials and reagents, such as carbon-based/graphene-based composite adsorbents [7–11], metal–organic frameworks (MOFs)/nano adsorbents [5, 12], industrial and agricultural waste-based and natural minerals/polymers-based adsorbents [13–18] and so on. However, some powdered adsorbents are not easy to be thoroughly separated after wastewater treatment, resulting in partial loss and possible secondary pollution, and some

✉ Beigang Li
libeigang_1964@126.com; libg@imnu.edu.cn

[1] Chemistry & Environment Science College, Inner Mongolia Normal University, Hohhot 010022, China

[2] Inner Mongolia Key Laboratory of Environmental Chemistry, Inner Mongolia Normal University, Hohhot 010022, China

adsorbents are difficult to be popularized in application due to high price and insufficient decontamination performance. Hence, developing low-cost, eco-friendly, high-capacity and swift-separation adsorbents have become the key to the efficient implementation of adsorption technology [12, 16].

Sodium alginate (SA), a natural polysaccharide polymer with rich marine sources, excellent biocompatibility, nontoxicity and biodegradability, has been widely used in food, drugs, textile, printing and dyeing, paper products and other industrial production and has been payed close attention as a low-cost biomass material over recent years [19]. Currently, SA has frequently been prepared into various gel composites with great modification space as bio-based adsorbents by utilizing its strong hydrophilicity, gelation, polymerization property and high chemical reactivity, and applied to the high-efficiency pollutants removal from industrial wastewater. In particular, SA can be crosslinked by suitable polyvalent metal ions to form polymer macrogel particles with controllable chemical and mechanical properties, which are ideal skeletons for preparing composite macrospheres with stronger adsorption properties [19, 20]. For example, rare earth Y(III) ions can easily crosslink with SA and form uniform macrogel particles with ultralarge adsorption capacity owing to its unique electron shell structure and high positive charge [17, 21]. Recently, magnetic composites, as promising adsorbents, have been widely developed because of their rapid separation and recovery from treated water by external magnetic field to solve the problem of incomplete separation of some powder adsorbents [5, 16, 22].

Based on the previous research and above analysis [21], our study purpose has been not only to make full use of the high polymerization activity of rare earth ions with SA, but also to reduce the preparation cost of adsorbents and improve the overall efficiency of gel beads as much as possible. Therefore, a novel magnetic macrogel copolymer (Fe-SA-Y@Fe_3O_4) with biosafety was further prepared by a facile co-crosslinking polymerization of Y(III) and Fe(III) ions with SA and Fe_3O_4 to reduce the amount of rare earth Yttrium and dramatically improve the adsorption capacity, stability and mechanical properties of the macrogel composite, and reach the rapid separation from treated wastewater. Taking DR 13 and DB 19 dyes as adsorption objects, important preparation and adsorption conditions, adsorption dynamics and thermodynamics of Fe-SA-Y@Fe_3O_4 composite for the target pollutants were investigated and its adsorption efficiency was evaluated. The dye-removed mechanism was explored. We hope to utilize natural biological resources to prepare cost-effective and eco-friendly macroparticle adsorbents with superlarge adsorption capacities and magnetic separation properties by a simple and feasible method, and realize the effective utilization of natural resources and ultra-efficient purification of azo dye wastewater.

Material and Methods

Chemicals and Materials

$FeCl_3{\cdot}6H_2O$ (AR), $Y(NO_3)_3{\cdot}6H_2O$ (AR), Fe_3O_4 (AR) and sodium alginate (SA, AR) were purchased from Damao Chemical Reagent Factory (Tianjin, China). Direct Red 13 (DR 13, $C_{32}H_{22}N_6Na_2O_7S_2$, $M_r = 712.66$ g/mol, $\lambda_{max} = 510$ nm) and Direct Black 19 (DB 19, $C_{34}H_{27}N_{13}Na_2O_7S_2$, $M_r = 839.77$ g/mol, $\lambda_{max} = 644$ nm) dyes were supplied by Jiaying Chemical Co., Ltd. (Shanghai, China), and dye molecular structures are shown in Fig. 1.

Synthesis of Fe-SA-Y@Fe_3O_4 Gel Composite

Fe-SA-Y@Fe_3O_4 gel composite was synthesized by a facile droplet polymerization, and the specific preparation process was as follows: 0.1 g Fe_3O_4 was added into 25 mL SA solution of 16 g/L with uniform stirring and ultrasonicated for 0.5 h at 25 ℃, and then dripped evenly into the 30 g/L mixed solution of Fe(III) and Y(III) ions with a mass ratio (m_{Fe}: m_Y) of 2:1 by a syringe with 0.45 mm diameter. Black

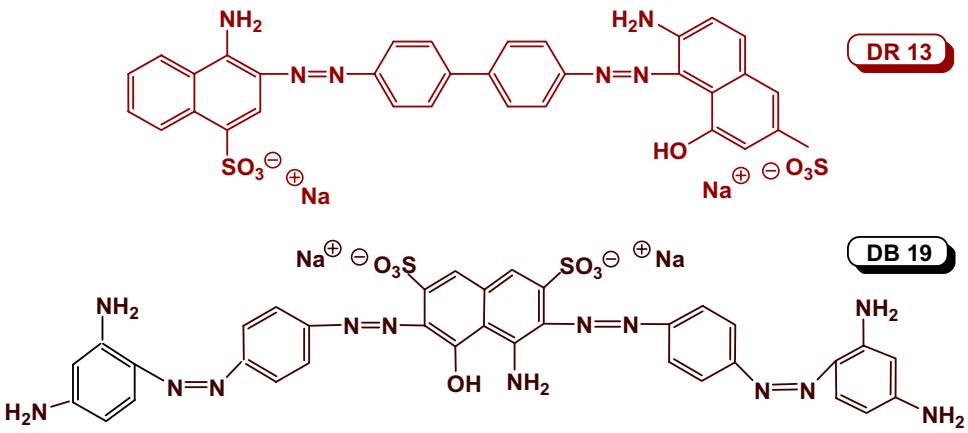

Fig. 1 Molecular structures of DR 13 and DB 19 dyes

spherical beads were observed to produce continuously. After curing for 3 h, the macrogel beads were removed, washed and dried, and magnetic bio-based adsorbent Fe-SA-Y@Fe_3O_4 was finally obtained for further study.

Characterization

Scanning electronic microscopy and energy dispersive spectroscopy (SEM–EDS, SU8010, Hitachi Inc., Japan) were used to examine the micromorphology and elemental distribution of samples. Crystal structure of raw materials and the gel composite was analyzed by a X-ray diffractometer (XRD, PW-1830, Philips, Holland) using Cu-Kα radiation source ($\lambda = 0.154056$ nm). Fourier transform infrared (FTIR) spectra were measured by a FTIR spectrometer (KBr tabletting method, Nicolet 6700, Thermo Fisher Scientific, U.S.A). The magnetic property of the composite was determined on a vibrating sample magnetometer (VSM, 7407, Lake Shore Inc., USA). XPS analysis was performed on an x-ray photoelectron spectroscopy (XPS) with a monochromatized Al Ka X-ray source (Axis Ultra, Shimadzu Inc., Japan).

Batch Adsorption Tests

All adsorption experiments for DR 13 and DB 19 removal from aqueous solutions by Fe-SA-Y@Fe_3O_4 gel beads were completed. Effects of initial dye concentration and solution pH on the dye adsorption were examined by adding 0.03 g dried gel beads into 25 mL dye solution with definite dye concentration and shaking for 60 min at 298 K. Similarly, the kinetic experiments affected by time and temperature, isothermal adsorption were further finished by batch adsorption experiments. After adsorption, each supernatant was separated, and then the residual dye concentration was determined by UV–vis spectrophotometry at λ_{max} of each dye, respectively. The amount (Q_t and Q_e, mg/g) and removal efficiency (R, %) of each dye adsorbed by the composite at contact time t (min) and equilibrium were calculated by the following equations, respectively:

$$Q_t \left(or\, Q_e\right) = (C_0 - C_e) \times V/W \tag{1}$$

$$R = (C_0 - C_e)/C_0 \times 100\% \tag{2}$$

where C_0 and C_e (mg/L) are the dye concentrations before and after adsorption, respectively. V (L) and W (g) are the solution volume and adsorbent dosage, respectively.

The adsorption experiments of each sample were repeated at least three times and the determined mean value was used for result analysis, and the precision of each-group data was controlled within the relative standard deviation (*RSD*) less than 2%.

Different Models and Formulas Used in Data Analysis

In order to clarify the adsorption rate and control its key step in the adsorption processes, to judge the adsorption performance of Fe-SA-Y@Fe_3O_4 composite for azo dyes and study deeply the dye adsorption behavior and interaction mechanism, the used different models and equations are listed in Table 1.

Table 1 Different models and equations used in data analysis

Names of various models and equations		Mathematical expression		Ref
Adsorption kinetics	Pseudo-first-order	$\log(Q_{e,\exp} - Q_t) = \log Q_{e,calc} - k_1 t$	(3)	[23]
	Pseudo-second-order	$t/Q_t = 1/(k_2 Q_{e,calc}^2) + t/Q_{e,calc}$	(4)	[24]
	Intraparticle diffusion	$Q_t = K_{id} t^{0.5} + C$	(5)	[25]
Isothermal adsorption	Langmuir	$C_e/Q_e = C_e/Q_m + 1/(Q_m K_L)$	(6)	[13]
	Freundlich	$\log Q_e = 1/n \log C_e + \log K_F$	(7)	
	Dubinin-Radushkevich (D-R)	$\ln Q_e = \ln Q_m - \beta\varepsilon^2$	(8)	
		$\varepsilon = RT \ln(1 + 1/C_e)$	(9)	
		$E = 1/\sqrt{-2\beta}$	(10)	
Thermodynamic study	Van't Hoff equation	$\Delta G^\circ = -RT \ln K^0$	(11)	[26]
		$\ln K^0 = \Delta S^\circ/R - \Delta H^\circ/RT$	(12)	

k_1 (min^{-1}) and k_2 [g/(mg·min)]: the rate constants of pseudo-first-order and pseudo-second-order models; K_{id} [mg/(g·$min^{1/2}$)]: the intraparticle diffusion rate constant; C: the thickness of the boundary layer; T(K): the absolute temperature; R [8.314 J/(mol·K)]: the gas constant; Q_m (mg/g): the maximum adsorption capacity; K_L (L/mg): the Langmuir adsorption constant; K_F and n: the Freundlich empirical constants; E (kJ/mol): the mean adsorption energy; β (mol^2/kJ^2): a constant related to adsorption energy; ε (kJ/mol): the Polanyi potential; K^0 ($= 1000 K_L M_{dye}$ dimensionless): the adsorption standard equilibrium constant; ΔG° (kJ/mol): Gibbs free energy change; ΔH° (kJ/mol) and ΔS° (kJ/mol·K): the enthalpy change and entropy change

Results and Discussion

Optimization of Preparation Conditions for Fe-SA-Y@Fe_3O_4 Gel Composite

As a crosslinking agent of SA-based composites, the proportioning of Fe(III) and Y(III) double ions is a key factor to form stable macrogel bead polymer. When the concentrations of SA solution and mixed solution of Fe(III) and Y(III) ions were fixed at 16 and 10 g/L respectively, ion-mixed solutions with different ion mass ratios (m_{Fe}: m_Y) were used for the synthesis of Fe-SA-Y polymer at room temperature, and the obtained polymer was further applied to the adsorption of DR 13 and DB 19 dyes respectively. As shown in Fig. 2(a and b), the adsorption amounts of DR 13 and DB 19 onto Fe-SA-Y polymers prepared by dual-ion polymerization were obviously higher than those onto Fe-SA and Y-SA polymer crosslinked by a single metal ion with SA. Moreover, the dye adsorption amounts and removal rates reached the maximum values with 1247 mg/g and 95.9% for DR 13 and 1371 mg/g and 97.9% for DB 19 respectively when the dual-ion mass ratio (m_{Fe}: m_Y) was 2:1, indicating that the Fe-SA-Y polymer prepared by dual-ion co-crosslinking SA has extremely significant improvement on the adsorption efficiency of azo dyes from the water. Hence, the mass ratio of m_{Fe}: $m_Y = 2{:}1$ was chosen to prepare Fe-SA-Y gel composite.

When the SA concentration and dual-ion mass ratio were 16 g/L and 2:1, the adsorption performance of different Fe-SA-Y polymers synthesized by changing total ion concentration (C_{Fe+Y}, g/L) for two dyes are presented in Fig. 2c. When the total ion-mixed concentration increased from 5 to 30 g/L, the adsorption amounts (Q_e, mg/g) of DR 13 and DB 19 by Fe-SA-Y increased dramatically from 676 and 531 mg/g to 1694 and 1841 mg/g and the removal rates (R, %) also increased rapidly from 39.5 and 28.6% to 98.8 and 99.1%, respectively, indicating that each dye was almost completely removed from wastewater. After that, the Q_e (mg/g) and R (%) values of DR 13 and DB 19 were unchanged nearly with keeping on increasing the ion-mixed concentration. Therefore, the 30 g/L concentration of Fe(III) and Y(III) ion-mixed solution was selected for preparing Fe-SA-Y polymer.

In preparing process of Fe-SA-Y polymer, Fe_3O_4 was further added to obtain the magnetic Fe-SA-Y@Fe_3O_4 composite, and effect of Fe_3O_4 concentration on adsorption properties of Fe-SA-Y@Fe_3O_4 for azo dyes were explored. As shown in Fig. 2d, Fe-SA-Y@Fe_3O_4 prepared by 4.0 g/L of Fe_3O_4 solution had the best adsorption effect and good magnetic separation performance confirmed by the actual magnetic separation tests, and higher adsorption capability than Fe-SA-Y polymer for two dyes. The influence of curing time on the stability and integrity of formed gel composite after crosslinking polymerization was presented in Fig. 2e. The Q_e (mg/g) and R (%) values of DR 13 and DB 19 onto Fe-SA-Y@Fe_3O_4 went up rapidly with curing time from 2 to 3 h, and then changed little with time extension. Consequently, 3 h of the curing time was selected by comprehensive consideration. In addition, the effect of crosslinking temperature on Fe-SA-Y@Fe_3O_4 properties was also examined. As given in Fig. 2f, the adsorption efficiency of two dyes onto Fe-SA-Y@Fe_3O_4 only fluctuated in varying degrees with a rise of crosslinking temperature from 25 to 55 ℃, but 25 ℃ was the best temperature of the composite preparation, which was also the best choice for convenient operation and energy conservation for practical application.

Material Characterization

As shown in the SEM micrographs of Fig. 3(a and b), the dried black Fe-SA-Y@Fe_3O_4 macrogel beads synthesized by milky-white powder SA exhibit a unique cauliflower-like surface with grooves and crevices of different depths and uneven shape, which is very favorable for reinforcing the adsorption properties of gel composite. Concurrently, some white particles were found to be dispersed on the surface of gel beads, which should be Fe_3O_4 particles. The same phenomena were also observed in the previous reports [27, 28]. Furthermore, according to the EDS results of element distribution presented in Fig. 3(c and d), the contents of Fe and Y undetected in SA were 26.1 and 5.4% in Fe-SA-Y@Fe_3O_4 respectively, and 11.0% of the Na content in SA reduced dramatically to 0.34% in the composite. The element distribution including C, O, Fe, Y and Na in gel beads was also very uniform (Fig. 3e–j) and a small part of Fe-element aggregation was observed (Fig. 3k), which was consistent with the white spots in SEM images. These results fully indicated that ion exchange reaction between Fe(III)-Y(III) dual-ions and Na^+ ions in SA solution first occurred, and then the magnetic gel beads with so-called "egg-box" structure were successfully synthetized by crosslinking polymerization of dual ions with SA molecular chains [29].

In the XRD patterns of Fig. 3l, three diffraction peaks (2θ: 13.7°, 21.7° and 37.8°) on the SA curve [11, 21] almost disappeared on the XRD pattern of Fe-SA-Y@Fe_3O_4 [29], but the typical diffraction peaks at 2θ of 30.34°, 35.64°, 53.60°, 57.34° and 62.94° appeared, which should belong to the characteristic peaks of Fe_3O_4 [20], confirming the successful synthesis of Fe-SA-Y@Fe_3O_4 composite. It was known from the magnetic hysteresis loop of Fig. 3m that the saturation magnetization value of Fe-SA-Y@Fe_3O_4 was 7.06 emu/g. Meanwhile, the experimental test illustrated that

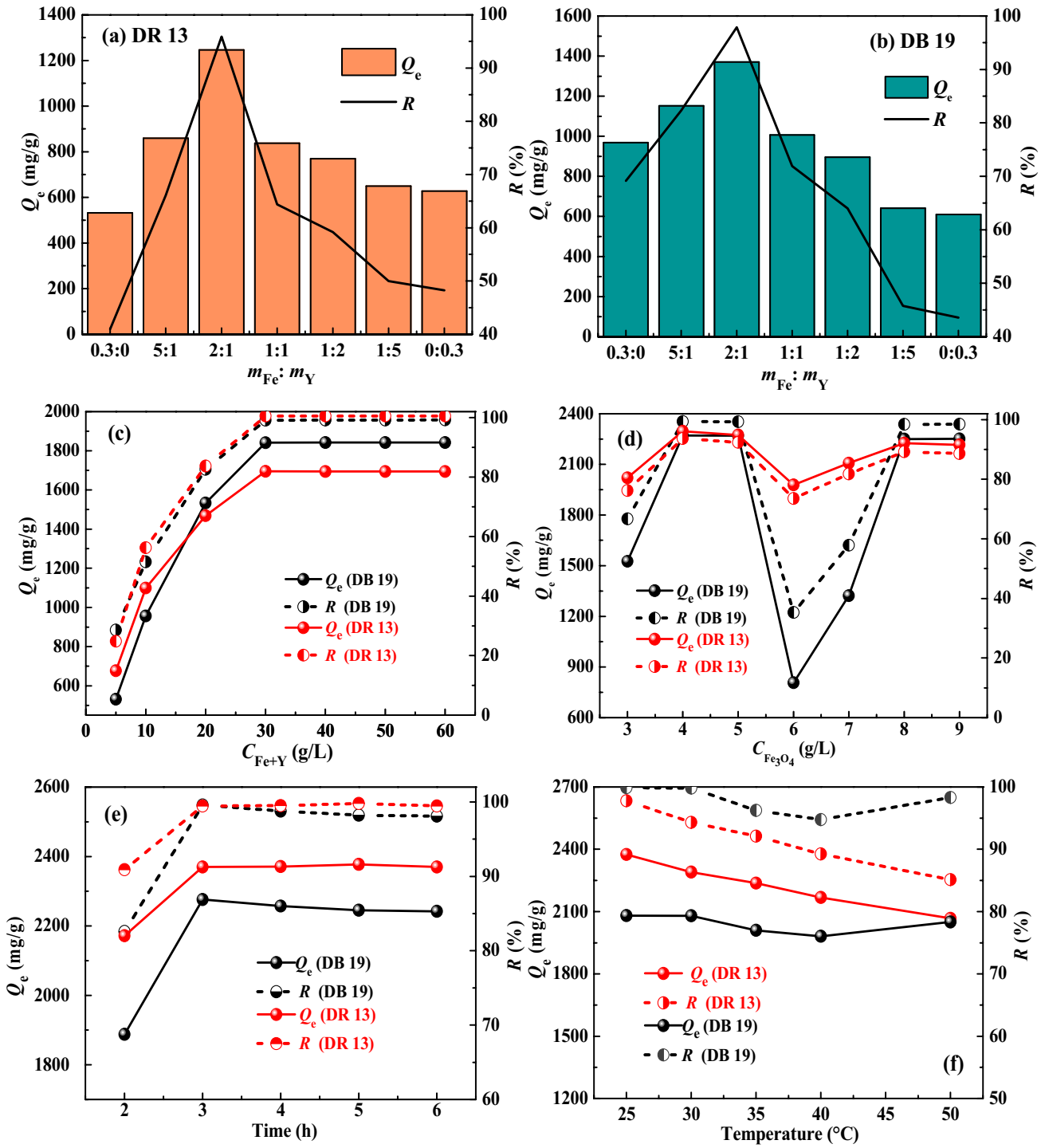

Fig. 2 Effect of double ion mass ratio (**a**, **b**), total concentration of double ions (**c**), Fe_3O_4 concentration (**d**), curing time (**e**) and crosslinking reaction temperature (**f**) on the adsorption amounts and removal rates (2600 and 2800 mg/L of DR-13 and DB-19 dye concentration, 60 min of adsorption time)

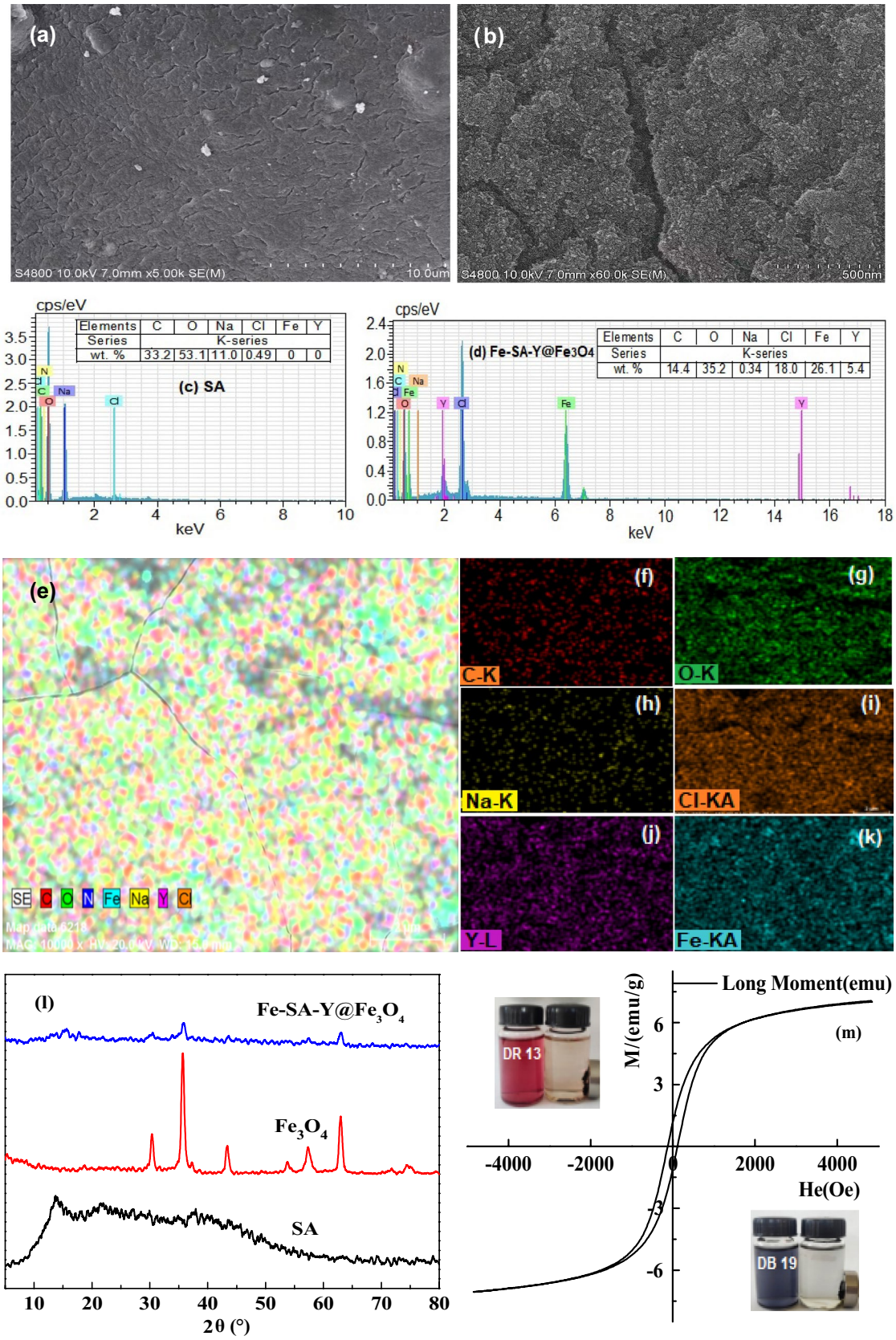

Fig. 3 SEM images of Fe-SA-Y@Fe_3O_4 (**a**, b); EDS results (**c**, **d**) of SA and Fe-SA-Y@Fe_3O_4 and element distribution (**e**–**k**) of the composite; XRD patters of samples (**l**); (**m**) Magnetic hysteresis loop of Fe-SA-Y@Fe_3O_4

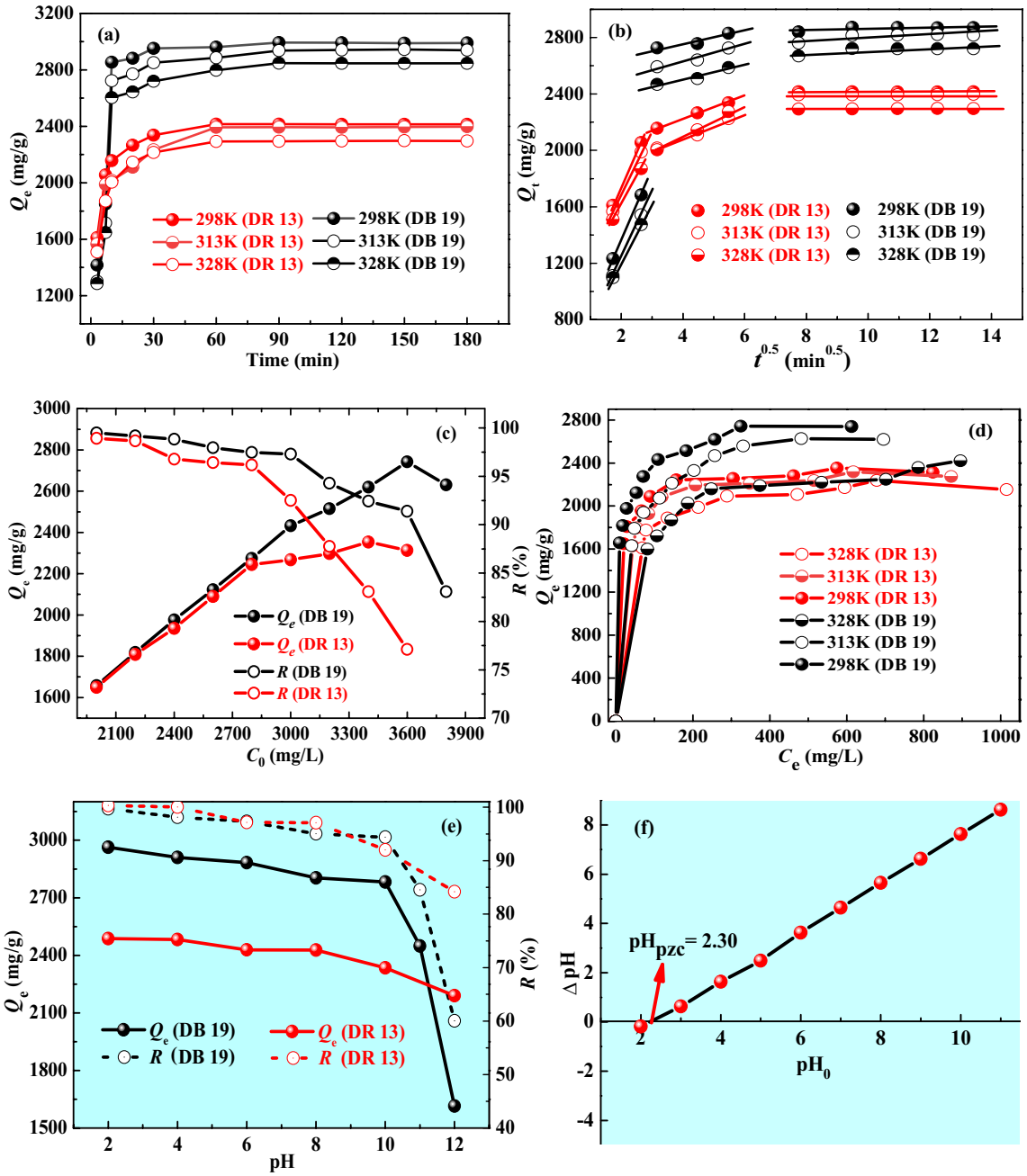

Fig. 4 (**a**) Effect of contact time and temperature on dye adsorption, (**b**) The plots of Q_t versus $t^{0.5}$, (**c**) Effect of initial dye concentration on the adsorption, (**d**) Adsorption isotherms of two dyes on Fe-SA-Y@Fe_3O_4, (**e**) Effect of solution pH on dye adsorption, (**f**) Determination of the composite pH_{pzc}

a small permanent magnet was placed on a bottle wall, and dye-adsorbed gel beads in the bottle were instantly assembled onto the wall (Fig. 3m), proving that Fe-SA-Y@Fe_3O_4 has the sensitive magnetic response property and can be quickly separated from treated water by a external magnetic field without secondary pollution and adsorbent loss.

Effect of Contact Time and Temperature and Adsorption Kinetics

When adsorption technology is used for wastewater treatment, the adsorption-required equilibrium time and temperature will directly determine the actual investment, application cost and treatment efficiency. The adsorption amounts (Q_t) of DR 13 and DB 19 onto Fe-SA-Y@Fe_3O_4 at 298 K dramatically increased in 10 min of contact time, and then increased slowly with time increase in Fig. 4a. The adsorption equilibrium of each dye could be reached within 90 min, and the corresponding Q_t value was up to 2416 and 2856 mg/g for DR 13 and DB 19, respectively. The adsorption rate of each dye concurrently descended with temperature increase from 298 to 328 K, but the temperature had no effect on the time required for reaching adsorption equilibrium. The results indicate that Fe-SA-Y@Fe_3O_4 gel composite with the fast adsorption equilibrium and ultrahigh adsorption amounts, as a very potential bio-based adsorbent, has the best decolorization effect on azo dye wastewater at room temperature.

To describe the dynamic processes of adsorption systems well and clarify the control step of adsorption rate, the pseudo-first-order and pseudo-second-order rate models and intraparticle diffusion model were respectively used to analyze kinetic data of each dye adsorption onto Fe-SA-Y@Fe_3O_4 in the light of Eqs. (3, 4, 5) in Table 1, and the goodness-of-fit of rate models to the experimental data was evaluated by calculating relative error (RE, %) = $(Q_{e,exp}\text{-}Q_{e,calc})/Q_{e,exp}$ 100 [30]. The fitting results in Table 2 elucidated that the kinetic data for each dye adsorption at different temperatures were completely consistent with the pseudo-second-order model (the correlation coefficient $R^2 \geq 0.999$), and had more perfect goodness-of-fit (RE: − 6.9 to − 0.78%) for the pseudo-second-order model than the pseudo-first-order model ($R^2 \geq 0.745$; RE: 90 – 69%). The calculated $Q_{e,2}$ values were very close to those of experimental $Q_{e,exp}$, suggesting the occurrence of chemisorption [31]. Moreover, a reduction in pseudo-second-order rate constant (k_2) with temperature increase indicated the exothermic adsorption. Similar phenomenon has also been reported [28].

Table 2 Kinetic fitting results of dye adsorption onto the gel composite by different models

Dyes	T (K)	$Q_{e,exp}$ (mg/g)	Pseudo-first-order			RE (%)
			k_1 (min^{-1})	$Q_{e,1}$ (mg/g)	R_1^2	
DR 13	298	2416	0.0161	244	0.745	90
	313	2398	0.0183	457	0.839	81
	328	2297	0.0192	278	0.840	88
DB 19	298	2856	0.0142	431	0.774	85
	313	2798	0.0145	585	0.803	79
	328	2683	0.0193	825	0.902	69
Dyes	T (K)	$Q_{e,exp}$ (mg/g)	Pseudo-second-order			RE (%)
			k_2 [g/(mg·min)]	$Q_{e,2}$ (mg/g)	R_2^2	
DR 13	298	2416	0.000423	2433	1.000	-6.9
	313	2398	0.000265	2421	1.000	-1.0
	328	2297	0.000413	2315	1.000	-0.78
DB 19	298	2856	0.000141	2907	1.000	-1.8
	313	2798	0.000112	2857	1.000	-2.1
	328	2683	0.000101	2747	0.999	-2.4
Dyes	T (K)	Intraparticle diffusion model				
		First stage		Second stage		Third stage
		K_{id}(mg/g·$min^{1/2}$)	R^2	K_{id}(mg/g·$min^{1/2}$)	R^2	Balance stage
DR 13	298	394	1.000	43.7	0.996	Upper platforms on fitting curves
	313	331	1.000	84.6	0.964	
	328	351	1.000	38.6	0.999	
DB 19	298	561	1.000	49.2	0.902	
	313	535	1.000	64.6	0.950	
	328	469	1.000	57.5	0.937	

The whole process of dye adsorption is usually divided into three steps: liquid film diffusion, pore diffusion and physicochemical adsorption onto adsorbent surface [32]. In this study, all kinetic experimental data were further processed using the intraparticle diffusion model (Eq. 5 in Table 1) for grasping a key step to control the adsorption rate [25]. According to the results in Fig. 4b and Table 2, the initial fast stages and second slow stages in the adsorption process of each dye onto the gel beads were primarily controlled by the intraparticle diffusion (pore diffusion), but were not the only one.

Effect of Dye Concentration and Adsorption Isotherms

The influence of initial dye concentration (C_0) on the adsorption capacities (Q_e) of the gel composite is given in Fig. 4c. When the initial concentration of DR 13 solution increased from 2000 to 3400 mg/L, the Q_e (mg/g) value increased from 1649 to 2354 mg/g while R (%) value decreased slightly from 98.9 to 83.1%. Similarly, the Q_e value of DB 19 increased from 1658 to 2742 mg/g while R (%) value only decreased a little from 99.5 to 91.4% with a rise in the initial concentration from 2000 to 3600 mg/L. This is due to the rapid mass transfer of dye anions with high contents in the solution and the sufficient number of active sites on the adsorbent surface, but R (%) value reduced gradually with the saturation of active sites. Further studies showed that the Q_e value of each dye diminished with increasing in temperature from 298 to 328 K in the absorption isotherms of Fig. 4d, which were in line with the impact results of temperature on dye adsorption kinetics. The isothermal data of each dye adsorption onto Fe-SA-Y@Fe_3O_4 at different temperatures were respectively handled with Langmuir, Freundlich and Dubinin-Radushkevich (D-R) models (Eqs. 6–10 in Table 1), and the results are shown in Table 3. By comparing the correlation coefficient (R^2) for fitting three models, the equilibrium data were most consistent with the Langmuir model ($R^2 \geq 0.998$) and the fitting result owned the more significant goodness-of-fit (root mean squared error: RMSE $\leq 5.9\times10^{-3}$) than the Freundlich model ($R^2 \geq 0.849$; RMSE $\leq 2.2\times10^{-2}$) at each temperature [33]. The maximum Q_m value of each dye was very near the actual equilibrium $Q_{e,exp}$ (Table 2), demonstrating the occurrence of monolayer adsorption. Hence, the Langmuir model can describe the dye adsorption behavior well. Some adsorption studies obtained similar results [8, 21]. In general, the mean adsorption energy (E) from D-R model with the range of 1 – 8 kJ/mol and more than 8 kJ/mol can predict the occurrence of physical adsorption or chemical adsorption, respectively [34]. The E values of DR 13 and DB 19 adsorption, from 23.4 to 22.3 kJ/mol and from 8.98 to 7.42 kJ/mol at 298 – 328 K, respectively, revealed the mechanism involving the chemisorption and micropore filling. The Langmuir constant (K_L) and Freundlich constant (K_F) related to adsorption strength and affinity reduced with temperature increasing from 298 to 328 K, suggesting the exothermic nature of adsorption systems and confirming that the room temperature could better enhance the adsorption and be more convenient for practical application.

The maximum adsorption capacities of different direct dyes onto various adsorbents previously reported are listed in Table 4. Quite evidently, as a eco-friendly bio-based adsorbent, Fe-SA-Y@Fe_3O_4 gel beads with the magnetism

Table 3 Fitting results of three isotherm models for equilibrium data and thermodynamic parameters of dye adsorption onto the gel composite

Dyes	T (K)	Langmuir model				Freundlich model			
		Q_m (mg/g)	K_L (L/mg)	R^2	RMSE	$1/n$	logK_F	R^2	RMSE
DR 13	298	2353	0.0977	1.000	2.1×10^{-3}	0.089	3.13	0.893	1.9×10^{-2}
	313	2331	0.0622	1.000	2.6×10^{-3}	0.102	3.08	0.849	2.2×10^{-2}
	328	2232	0.0459	0.999	5.1×10^{-3}	0.105	3.04	0.874	1.8×10^{-2}
DB 19	298	2793	0.0745	0.999	1.8×10^{-3}	0.130	3.10	0.970	1.5×10^{-2}
	313	2755	0.0324	0.999	2.0×10^{-3}	0.170	2.96	0.948	1.8×10^{-2}
	328	2488	0.0211	0.998	5.9×10^{-3}	0.151	2.94	0.908	1.9×10^{-2}
Dyes	T (K)	Dubinin-Radushkevich (D-R) model					Thermodynamic parameters		
		Q_m (mg/g)	$\beta\times10^{-3}$ (mol^2/kJ^2)	E (kJ/mol)	R^2	RMSE	$\Delta G°$ (kJ/mol)	$\Delta H°$ (kJ/mol)	$\Delta S°$ (kJ/mol·K)
DR 13	298	3150	− 0.913	23.4	0.962	5.2×10^{-2}	− 27.6	− 20.5	0.0237
	313	3334	− 1.04	21.9	0.929	2.9×10^{-2}	− 27.9		
	328	3212	− 1.01	22.3	0.937	3.4×10^{-2}	− 28.3		
DB 19	298	4352	− 6.20	8.98	0.981	1.1×10^{-1}	− 27.2	− 34.3	− 0.0238
	313	5021	− 1.85	16.4	0.982	6.9×10^{-2}	− 26.9		
	328	2261	− 9.09	7.42	0.971	4.5×10^{-2}	− 26.5		

Table 4 Comparison of the maximum adsorption capacities (Q_m) of direct dyes onto various adsorbents

Adsorbent	Dye	Q_m (mg/g)	Ref
α-CDs-EPI	Direct Red 83:1	31.50	[35]
HP-α-CDs-EPI	Direct Red 83:1	23.41	
Bamboo sawdust	Direct red 81	6.43	[36]
Treated bamboo sawdust	Direct red 81	13.83	
Polyacrylamide/activated carbon	Direct red 80	162.0	[37]
Gelatin-CNT-MNPs	Direct red 80	380.7	[22]
Fe_3O_4-N-GO@SA	Direct red 28 (Congo red)	30.06	[12]
PS-CS	Direct red 28 (Congo red)	1081.1	[38]
N_U-UiO-67	Direct red 28 (Congo red)	2360	[39]
N_T-UiO-67	Direct red 28 (Congo red)	1986	
N_A-UiO-67	Direct red 28 (Congo red)	1493	
Magadiite-chitosan composite beads	Direct red 28 (Congo red)	200	[33]
APEADA (resin)	Direct red 28 (Congo red)	280	[40]
Fe_3O_4@ZTB-1	Direct red 28 (Congo red)	458	[5]
Fe(III)/Cs@Dia	Direct red 28 (Congo red)	1111	[13]
	Direct red 23 (Congo red)	1429	
	Direct yellow R	909.1	
	Direct orange 2GL	1250	
Graphene oxide (GO)	Direct red 23	15.3	[8]
Orange peel	Direct red 23	10.718	[41]
	Direct Red 80	21.052	
Biochar produced by the pyrolysis of pig manure	Direct red 23	17.32	[7]
Modified Gambir Adsorbent	Direct red 23	26.67	[42]
Powdered tourmaline (PT)	Direct red 23	153	[43]
CS/OSR/Silica hybrid membrane	Direct Red 31	94.4	[14]
	Direct Blue 71	67.2	
Y/CS/MFA	Direct green 6	627	[44]
Rice husk	Direct Red-31	25.63	[45]
	Direct Orange-26	19.96	
HCl treated rice husk	Direct Orange-26	24.22	[18]
	Direct Red-31	26.16	
	Direct Blue-67	19.85	
	Ever direct Orange-3GL	25.69	
Fe_3O_4@SA/Y	Direct Blue 86	370	[17]
	Direct Green 6	435	
	Direct Brown 2	1250	
CTAB–bentonite	Direct Red 2	153.84	[46]
ZAJHC ($ZnCl_2$ activated Jatropha husk carbon)	Direct Red 12B	39	[9]
Kaolinite	Direct Red 13	7.5	[15]
K-nZVI	Direct Fast Black G (Direct Black 19)	52.12	[47]
Fe-SA-Y@Fe_3O_4	Direct Red 13	2487	This study
	Direct Black 19	2992	

has outperformed many other adsorbents and displayed very significant advantages with ultrahigh adsorption efficiency, rapid separation and recovery after treating water. In addition, the adsorption capacity of Fe-SA-Y@Fe_3O_4 for DB 19 was larger than that for DR 13. This should be because there are more amino, azo and aromatic groups on the DB 19 molecules than those on DR 13 molecules (Fig. 1), resulting in more multisite interactions between the adsorbent and DB 19 molecules.

Adsorption Thermodynamics

According to Eqs. 11, 12 in Table 1, three thermodynamic parameters, the change of Gibbs free energy (ΔG°, kJ/mol), enthalpy change (ΔH°, kJ/mol) and entropy change (ΔS°, kJ/mol·K), were calculated to understand the feasibility and nature of adsorption reaction. The values of ΔH° and ΔS° obtained by the slope and intercept of the plot of $\ln K^0$ versus $1/T$ (DR 13: $\ln K^0 = 2.4671/T + 0.00285$, $R^2 = 0.993$; DB 19: $\ln K^0 = 4.1281/T$—0.00286, $R^2 = 0.976$) and ΔG° values are listed in Table 3. The negative values of ΔG° illustrated that the adsorption reactions were spontaneous and feasible. The negative values of ΔH° with − 20.5 kJ/mol (DR 13-Fe-SA-Y@Fe_3O_4) and − 34.3 kJ/mol (DB 19-Fe-SA-Y@Fe_3O_4) revealed the exothermic nature of dye adsorption. Some previous studies for azo dye adsorption also had similar results [21, 31]. A small positive value of ΔS° for DR 13 adsorption indicated the randomness increase at the solid–liquid interface due to the release of a large number of water molecules replaced by dye molecules, and also reconfirmed the good affinity of Fe-SA-Y@Fe_3O_4 for DR 13 [22, 40]. A negative ΔS° value of -0.0238 kJ/(mol·K) for DB 19 adsorption indicated the increase of dye-sorbed amount onto the composite and the enhancement of orderliness at the solid–liquid interface due to the monolayer adsorption [8, 13].

Effect of pH and Adsorption Mechanism

Wastewater pH can directly affect the treatment efficiency of adsorbent application. Therefore, the effects of pH on the DR 13 and DB 19 adsorption onto Fe-SA-Y@Fe_3O_4 were examined in detail. As presented in Fig. 4e, the Q_e values of DR 13 and DB 19 adsorbed decreased only slightly from 2487 to 2334 mg/g and from 2992 to 2831 mg/g when the pH of dye solution increased from 2.0 to 10.0, and the corresponding R(%) values reduced a little from 99.5 to 93.4% and from 99.7 to 94.4% respectively. After then the values of Q_e and R reduced with pH increase from 10.0 to 12.0. Meanwhile, the determined point of zero charge (pH_{pzc}) of Fe-SA-Y@Fe_3O_4 composite was 2.3 (Fig. 4f) [21], illustrating that the protonated positively charged surface of the gel composite promoted the adsorption of DR 13 and DB 19 anions by highly strong electrostatic attraction at $pH < pH_{pzc}$ [8], leading to the maximum adsorption capacities with 2487 and 2992 mg/g at pH 2.0 [36]. When solution pH was greater than pH_{pzc}, the deprotonated negative charge density of the composite surface increased with pH increasing and should lead to a remarkable decrease of adsorption capacity owing to the increase of electrostatic repulsion force between the adsorbent and dye anions [7], but actual adsorption results were not so (Fig. 4e), suggesting that there were still other interacting mechanism. The abundant O-containing functional groups including -COOH, -OH, M-OH (M: Fe^{3+} and Y^{3+}) and Fe–O (Fe_3O_4) on Fe-SA-Y@Fe_3O_4 surface easily formed various multi-site H-bonding interactions with -NH_2, -OH, -N = N-, -SO_3^- groups and -aromatic rings (Ar) in dye molecules, such as dipole–dipole H-bonding (O–H···N, O–H···O, O–H···S, M-OH···N) [12, 31, 40], Yoshida H-bonding (-COOH···Ar, -OH···Ar, M-OH···Ar) and n-π interaction (-COO^-···Ar, M–O···Ar) at higher pH [16], which effectively improved the removal efficiency of dyes. Meanwhile, the complexation might be another important mechanism due to the deprotonation of Fe-SA-Y@Fe_3O_4 polymer containing high-valence metals (Y^{3+} and Fe^{3+}) [29]. Concurrently, the unique cauliflower-like surface of gel beads with uneven three-dimensional structure was also very conducive to the rapid liquid film diffusion, pore migration and surface reaction of dye anions from the solution to the adsorbent inside. As a result, Fe-SA-Y@Fe_3O_4 gel composite has exhibited the ultrahigh adsorption capacity and nearly 100% removal efficiency for two dyes in a wide pH range of 2.0–10.0. The homologous results of some direct dyes adsorption affected by pH have also been found [44]. The values of Q_e (mg/g) and R (%) of the gel composite for DR 13 and DB 19 in each dye solution with a natural pH (8.0 and 9.0, respectively) could still achieve 2428 mg/g and 97.1%, and 2844 mg/g and 95.0%, respectively, so the gel composite can be directly applied to the superefficient treatment of dye wastewater without pH adjustment. This would be very favourable to reducing the cost of actual investment and simplifying the operation.

The FTIR spectra of Fe-SA-Y@Fe_3O_4 composite before and after dye adsorption were measured as shown in Fig. 5a, the positions and intensities of characteristic peaks at around 3395 (-OH), 1626 and 1383 (asymmetric and symmetric stretching vibration of -COO^-, respectively), 1027 (C–O–C) and 565 cm^{-1} (Fe–O) on the composite FTIR spectrum [20] all moved and changed correspondingly after adsorbing DR 13 and DB 19 respectively, confirming that the O-containing active groups and Fe_3O_4 on the composite participated in the interaction with dye anions.

Furthermore, the XPS wide-scan spectra of Fe-SA-Y@Fe_3O_4 before and after dye adsorption from Fig. 5b indicated that the gel composite mainly contained C, O, Fe and Y elements and the existence of Fe 2p peak derived from Fe_3O_4 confirmed successful synthesis of magnetic polymer [27]. Meanwhile, a new peak assigning to N 1 s appeared on the XPS spectra of DR 13-loaded and DB 19-loaded Fe-SA-Y@Fe_3O_4 respectively, illustrating that each dye was successfully bound to the gel composite. In the high-resolution XPS spectrum of C 1s (Fig. 5c), three peaks at binding energies of 284.7 (C – C), 285.1 (C-O, C – OH) and 288.6 eV (COO^-) [40] were shifted to 284.6, 285.5 and 287.6 eV after DR 13 adsorption, and 284.9, 286.1 and 288.8 eV after DB 19 adsorption, respectively, and all peak area ratios decreased. Two peaks with the binding

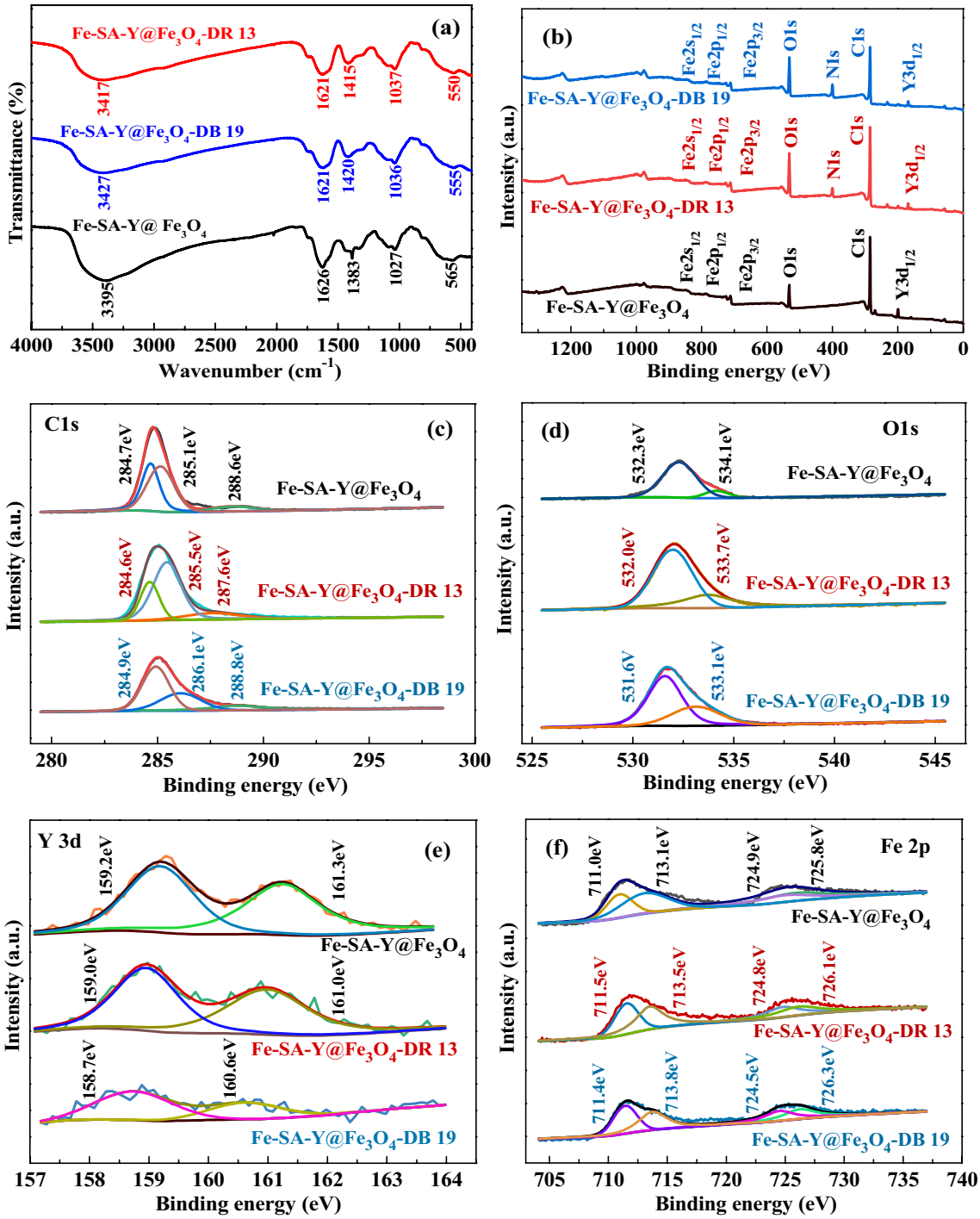

Fig. 5 FTIR (**a**) and XPS spectra (**b**–**f**) of the gel composite before and after dye adsorption

energy of 532.3 (C – OH, C–O–C) and 534.16 eV (COO^-, H–O-H: adsorbed water) [7, 14] on the O1s spectrum of the composite (Fig. 5d) were moved to 532.0 and 533.7 eV, and to 531.6 and 533.1 eV after adsorbing DR 13 and DB 19, respectively. The corresponding area ratios changed into 1:1.9 and 1:5.3, and 1:1.6 and 1:5.4, respectively. In the high-resolution XPS spectrum of Y 3d (Fig. 5e), two peaks assigned to Y $3d_{5/2}$ and Y $3d_{3/2}$ at 159.2 and 161.3 eV

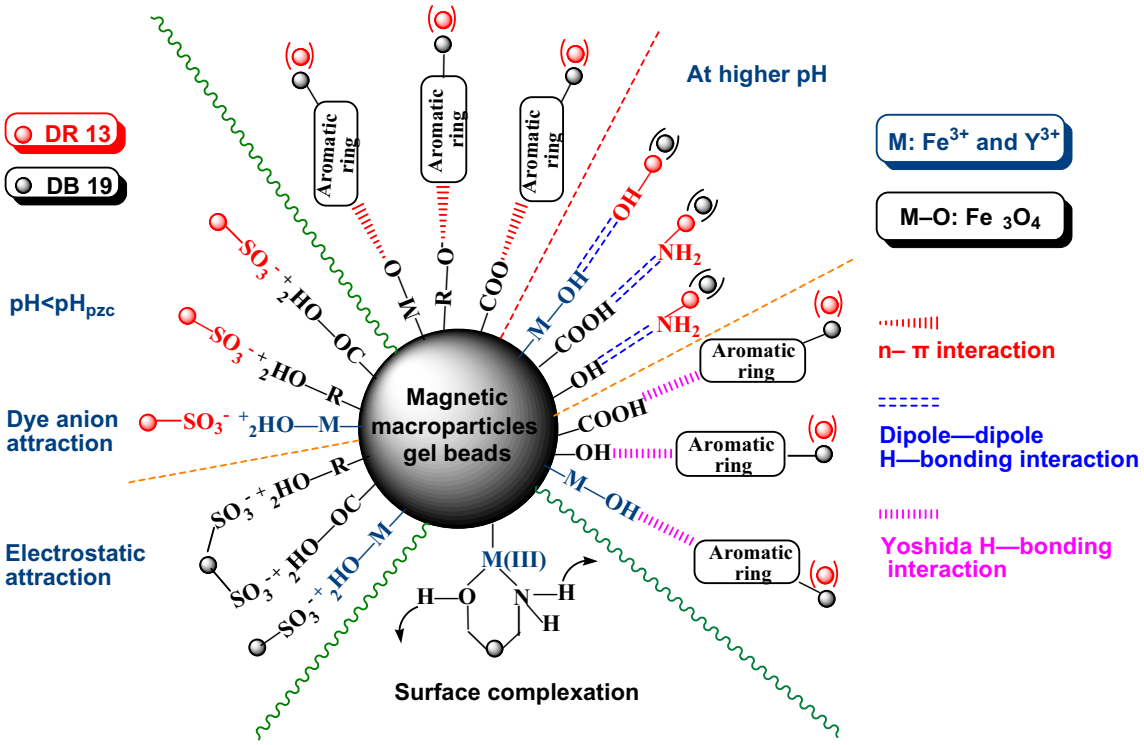

Fig. 6 Suggested interaction between the magnetic gel composite and direct dyes

demonstrated that the yttrium existed in the gel composite as Y(III) [48]. After adsorbing dyes, the binding energies of two peaks were slightly shifted to the low field direction with 159.0 and 161.0 eV for DR 13-loaded composite and 158.7 and 160.6 eV for DB 19-loaded composite, respectively, and corresponding area ratios decreased simultaneously, proposing that there was a complex reaction between Y(III) and dye anions. The spectra of Fe $2p_{3/2}$ and Fe $2p_{1/2}$ were respectively divided into four peaks at binding energies of 711.0, 713.1, 724.9 and 725.8 eV on the high-resolution spectrum of Fe 2p (Fig. 5f), proving the existence of Fe(III) with + 3 oxidation state and Fe_3O_4 in the gel composite [49]. However, after adsorbing dyes, the position and intensity of each peak for Fe 2p changed accordingly. All XPS results indicated that the various O-containing active groups, synergistic effect of bimetallic ions with the unsaturated coordination [29] and Fe_3O_4 in Fe-SA-Y@Fe_3O_4 polymer were all involved in the hydrogen bonding and coordination reactions with the rich -NH_2, -OH and azo groups as well as aromatic rings in dye anions, which further verified the FTIR results.

All results of material characterization, kinetic and thermodynamic studies and pH effect indicated that various interaction, mainly including electrostatic attraction, various H-bonding interaction and coordination reaction (Fig. 6), effectively promoted the strong multi-site adsorption between dyes and Fe-SA-Y@Fe_3O_4, resulting in the ultrahigh adsorption capacities of macrogel particles to two azo dyes.

Conclusion

Magnetic gel composite Fe-SA-Y@Fe_3O_4 synthesized by facile droplet polymerization using SA as raw material exhibits outstanding adsorption performance, and has maximum adsorption capacities of 2487 and 2992 mg/g for DR 13 and DB 19 at 298 K, respectively. The dye removal efficiency of almost 100% at pH 2.0 can still reach more than 94% with pH up to 10.0 (Fig. 7). The Pseudo-second-order rate model and Langmuir model can accurately describe the spontaneous adsorption processes with exothermic properties and adsorption behavior, respectively. As an eco-friendly, separable and high value-added bio-based adsorbent, macroparticle Fe-SA-Y@Fe_3O_4 gel composite would have considerable application potential for ultrastrong purification of azo-dye-containing effluents with various acidity.

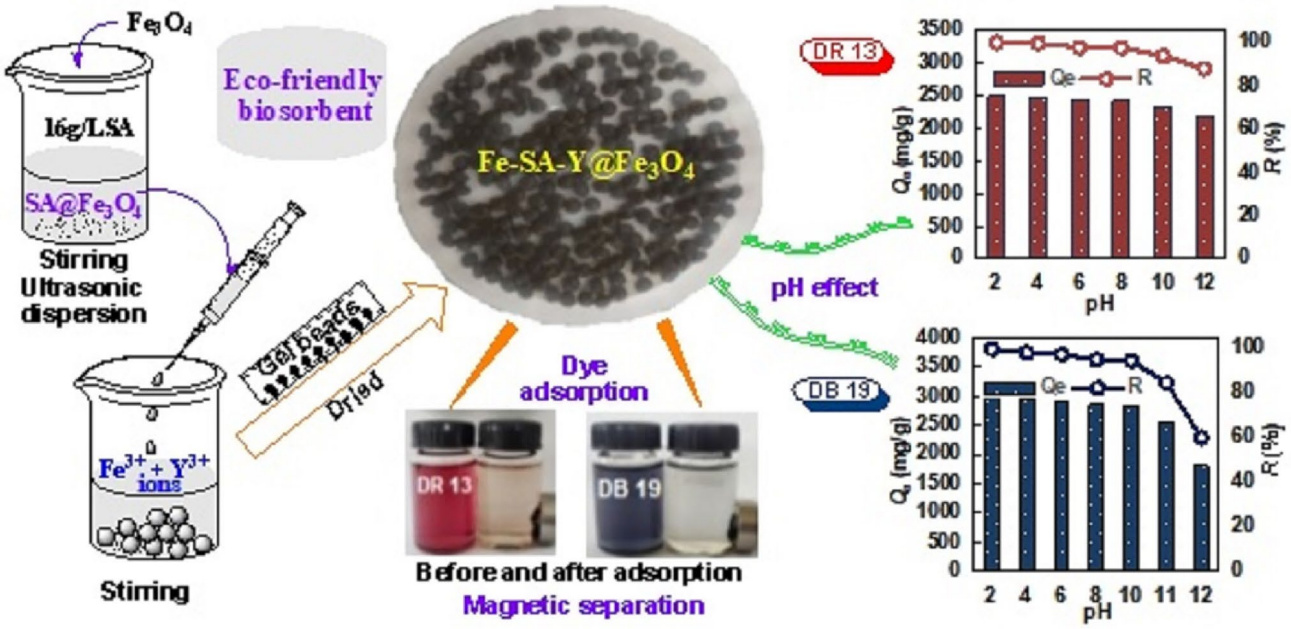

Fig.7 Schematic diagram of Fe-SA-Y@Fe_3O_4 gel composite from raw materials, preparation to adsorption application

Supplementary Information The online version contains supplementary material available at https://doi.org/10.1007/s10924-022-02404-6.

Acknowledgements This work was supported by the National Natural Science Foundation of China (21167011); the Natural Science Foundation of Inner Mongolia Autonomous Region, China (2020LH02009); and Collaborative Innovation Center for Water Environment Security of Inner Mongolia Autonomous Region, China (XTCX003).

Declarations

Conflict of interest The authors declare that they have no known competing financial interests or personal relationships that could have appeared to influence the work reported in this paper.

References

1. Lellis B, Fávaro-Polonio CZ, Pamphile JA, Polonio JC (2019) Effects of textile dyes on health and the environment and bioremediation potential of living organisms. Biotechnol Res Innovat 3:275–290. https://doi.org/10.1016/j.biori.2019.09.001
2. Pavithra KG, Jaikumar V (2019) Removal of colorants from wastewater: a review on sources and treatment strategies. J Ind Eng Chem 75:1–19
3. Sivashankar R, Sathya AB, Uma K, Sivasubramanian V (2015) Synthesis of magnetic biocomposite for effificient adsorption of azo dye from aqueous solution. Ecotoxicol Environ Saf 121:149–153
4. Brüschweiler BJ, Merlot C (2017) Azo dyes in clothing textiles can be cleaved into a series of mutagenic aromatic amines which are not regulated yet. Regul Toxicol Pharm 88:214–226
5. Han L, Ge F, Sun G, Gao X, Zheng H (2019) Effective adsorption of Congo red by a MOF-based magnetic material. Dalton Trans 48:4650–4656
6. Adeel S, Usman M, Haider W, Saeed M, Muneer M, Ali M (2015) Dyeing of gamma irradiated cotton using direct yellow 12 and direct yellow 27: improvement in colour strength and fastness properties. Cellulose 22:2095–2105
7. Liu N, Zhu M, Wang H, Ma H (2016) Adsorption characteristics of Direct Red 23 from aqueous solution by biochar. J Mol Liq 223:335–342
8. Konicki W, Aleksandrzak M, Moszyński D, Mijowska E (2017) Adsorption of anionic azo-dyes from aqueous solutions onto graphene oxide: Equilibrium, kinetic and thermodynamic studies. J Colloid Interf Sci 496:188–200
9. Karthick K, Namasivayam A, Pragasan LA (2017) Removal of Direct Red 12B from aqueous medium by $ZnCl_2$ activated Jatropha husk carbon: Adsorption dynamics and equilibrium studies. Indian J Chem Techn 24:73–81
10. Azari A, Nabizadeh R, Nasseri S, Mahvi AH, Mesdaghinia AR (2020) Comprehensive systematic review and meta-analysis of dyes adsorption by carbon-based adsorbent materials: classification and analysis of last decade studies. Chemosphere 250:126238
11. Mohammadi A, Doctorsafaei AH, Zia KM (2018) Alginate/calix[4]arenes modified graphene oxide nanocomposite beads: preparation, characterization, and dye adsorption studies. Int J Biol Macromol 20:1353–1361
12. Chen J, Hu H, Yang J, Xue H, Tian Y, Fan K, Zeng Z, Yang J, Wang R, Liu Y (2021) Removal behaviors and mechanisms for series of azo dye wastewater by novel nano constructed macroarchitectures material. Bioresour Technol 322:124556
13. Zheng L, Wang C, Shu Y, Yan X, Li L (2015) Utilization of diatomite/chitosan-Fe(III) composite for the removal of anionic azo dyes from wastewater: Equilibrium, kinetics and thermodynamics. Colloids Surf A: Physicochem Eng Aspect 468:129–139
14. He X, Du M, Li H, Zhou T (2016) Removal of direct dyes from aqueous solution by oxidized starch cross-linked chitosan/silica hybrid membrane. Int J Biol Macromol 82:174–181
15. Dhaif-Allah MAH, Syed AA (2018) Use of Kaolinite as an adsorbent: equilibrium and dynamics of adsorption of direct red 13

from aqueous solution. International Journal of Recent Scientific Research 9:28260–28269
16. Malek NNA, Jawad AH, Abdulhameed AS, Ismail K, Hameed BH (2020) New magnetic Schiff's base-chitosan-glyoxal/fly ash/Fe3O4 biocomposite for the removal of anionic azo dye: An optimized process. Int J Biol Macromol 146:530–539
17. Li B, Chen C (2021) Novel magnetic gel composite based on sodium alginate crosslinked by Yttrium(III) as biosorbent for efficient removal of direct dyes from aqueous solution. J Disper Sci Techno. https://doi.org/10.1080/01932691.2021.1924190
18. Bhatti HN, Safa Y, Yakout SM, Shair OH, Iqbal M, Nazir A (2020) Efficient removal of dyes using carboxymethyl cellulose/alginate/polyvinyl alcohol/rice husk composite: Adsorption/desorption, kinetics and recycling studies. Int J Biol Macromol 150:861–870
19. Ching SH, Bansal N, Bhandari B (2017) Alginate gel particles-a review of production techniques and physical properties. Crit Rev Food Sci Nutr 57:1133–1152
20. Li X, Qi Y, Li Y, Zhang Y, He X, Wang Y (2013) Novel magnetic beads based on sodium alginate gel crosslinked by zirconium(IV) and their effective removal for Pb^{2+} in aqueous solutions by using a batch and continuous systems. Bioresour Technol 142:611–619
21. Li B, Yin H (2020) Superior adsorption property of a novel green biosorbent Yttrium/Alginate gel beads for dyes from aqueous solution. J Polym Environ 28:2137–2148
22. Saber-Samandari S, Yekta H, Mohseni M (2017) Adsorption of anionic and cationic dyes from aqueous solution using gelatin-based magnetic nanocomposite beads comprising carboxylic acid functionalized carbon nanotube. Chem Eng J 308:1133–1144
23. Lagergren S (1898) About the theory of so-called adsorption of soluble substances. K Sven Vetenskapsakad Handl 24:1–39
24. Ho YS, McKay G (1999) Pseudo-second order model for sorption processes. Process Biochem 34:451–465. https://doi.org/10.1016/S0032-9592(98)00112-5
25. Weber WJ, Morris JC (1963) Kinetics of adsorption on carbon from solution. J Sanit Eng Div Am Soc Civ Eng 89:31
26. Milonjić SK (2007) A consideration of the correct calculation of thermodynamic parameters of adsorption. J Serb Chem Soc 72:1363–1367
27. Liang XX, Omer AM, Hu Z, Wang Y, Yu D, Ouyang X (2019) Effificient adsorption of diclofenac sodium from aqueous solutions using magnetic amine-functionalized chitosan. Chemosphere 217:270–278
28. Lv T, Li B (2021) Preparation of novel magnetic sodium alginate-ferric(III) gel beads and their super-efficient removal of direct dyes from water. J Polym Environ 29:1576–1590
29. Dong Y, Dong W, Cao Y, Han Z, Ding Z (2011) Preparation and catalytic activity of Fe alginate gel beads for oxidative degradation of azo dyes under visible light irradiation. Catal Today 175:346–355
30. Hu J, Dai W, Yan X (2016) Comparison study on the adsorption performance of methylene blue and congo red on Cu-BTC. Desalin Water Treat 57:4081–4089
31. Pan Y, Xie H, Liu H, Cai P, Xiao H (2019) Novel cellulose/montmorillonite mesoporous composite beads for dye removal in single and binary systems. Bioresour Technol 286:121366
32. Nethaji S, Sivasamy A (2011) Adsorptive removal of an acid dye by lignocellulosic waste biomass activated carbon: equilibrium and kinetic studies. Chemosphere 82:1367–1372
33. Mokhtar A, Abdelkrim S, Djelad A, Sardi A, Boukoussa B, Sassi M, Bengueddach A (2020) Adsorption behavior of cationic and anionic dyes on magadiite-chitosan composite beads. Carbohyd Polym 229:115399
34. Chen A-H, Chen S-M (2009) Biosorption of azo dyes from aqueous solution by glutaraldehyde-crosslinked chitosans. J Hazard Mater 172:1111–1121. https://doi.org/10.1016/j.jhazmat.2009.07.104
35. Pellicer JA, Rodríguez-López MI, Fortea MI, Gabaldón Hernández JA, Lucas-Abellán C, Mercader-Ros MT, Ferrándiz M (2018) Removing of Direct Red 83:1 using (- and HP-(-CDs polymerized with epichlorohydrin: kinetic and equilibrium studies. Dyes Pigm 149:736–746
36. Khan TA, Dahiya S, Ali I (2012) Removal of Direct Red 81 dye from aqueous solution by native and citric acid modified bamboo sawdust-kinetic study and equilibrium isotherm analyses. G U J Sci 25:59–87
37. Oladipo AA, Gazi M (2015) Microwaves initiated synthesis of activated carbon-based composite hydrogel for simultaneous removal of copper(II) ions and direct red 80 dye: A multi-component adsorption system. J Taiwan Inst Chem E 47:125–136
38. Liu M, Xie Z, Ye H, Li W, Shi W, Liu Y, Zhang Y (2021) Waste polystyrene foam-chitosan composite materials as high-efficient scavenger for the anionic dyes. Colloids Surf A: Physicochem Eng Aspect 627:127155
39. Dong X, Lin Y, Ma Y, Zhao L (2020) N-contaning UiO-67 derived multifunctional hybrid materials as highly effective adsorbents for removal of congo red. Inorg Chim Acta 510:119748
40. Waheed A, Mansha M, Kazi IW, Ullah N (2019) Synthesis of a novel 3,5-diacrylamidobenzoic acid based hyper-cross-linked resin for the efficient adsorption of Congo Red and Rhodamine B. J Hazard Mater 369:528–538
41. Ardejani FD, Badii KH, Limaee NY, Mahmoodi NM, Arami M, Shafaei SZ, Mirhabibi AR (2007) Numerical modelling and laboratory studies on the removal of Direct Red 23 and Direct Red 80 dyes from textile effluents using orange peel, a low-cost adsorbent. Dyes Pigm 73:178–185
42. Achmad A, Kassim J, Suan TK, Amat RC, Seey TL (2012) Equilibrium, kinetic and thermodynamic studies on the adsorption of direct dye onto a novel green adsorbent developed from Uncaria Gambir extract. J Phys Sci 23:1–13
43. Liu N, Wang H, Weng C-H, Hwang C-C (2018) Adsorption characteristics of Direct Red 23 azo dye onto powdered tourmaline. Arabian J Chem 11:1281–1291
44. Li B, Ren Z (2020) Superior adsorption of direct dye from aqueous solution by Y(III)-chitosan-doped fly ash composite as low-cost adsorbent. J Polym Environ 28:1811–1821
45. Safa Y, Bhatti HN (2011) Biosorption of Direct Red-31 and Direct Orange-26 dyes by rice husk: application of factorial design analysis. Chem Eng Res Des 89:2566–2574
46. Zohra B, Aicha K, Fatima S, Nourredine B, Zoubir D (2008) Adsorption of Direct Red 2 on bentonite modified by cetyltrimethylammonium bromide. Chem Eng J 136:295–305
47. Jin X, Chen Z, Zhou R, Chen Z (2015) Synthesis of kaolin supported nanoscale zero-valent iron and its degradation mechanism of Direct Fast Black G in aqueous solution. Mater Res Bull 61:433–438
48. Yu Y, Yu L, Sun M, Chen JP (2016) Facile synthesis of highly active hydrated yttrium oxide towards arsenate adsorption. J Colloid Interf Sci 474:216–222
49. Yamashita T, Hayes P (2008) Analysis of XPS spectra of Fe^{2+} and Fe^{3+} ions in oxide materials. Applied Surf Sci 254:2441–2449